Alignment Detection Technology of Chang'e-6 Primary Package Container

Guanyu Wang [1], **Shenyi Jin** [2], **Xiangjin Deng** [2] **and Yufu Qu** [1,*]

1 School of Instrument Science and Optoelectronic Engineering, Beihang University, Beijing 100191, China; sy2317307@buaa.edu.cn
2 Institute of Spacecraft System Engineering, China Academy of Space Technology, Beijing 100094, China; 13466576618@139.com (S.J.); dengxiangjin@sina.com (X.D.)
* Correspondence: qyf@buaa.edu.cn; Tel.: +86-13718169572

Abstract: The Chang'e-6 mission achieved the first successful sample collection and return from the Moon's far side. Accurate alignment detection of the primary packaging container is critical for the success of this mission, as it ensures proper retrieval of lunar soil. To address challenges such as complex backgrounds, uneven lighting, and reflective surfaces, this paper introduces an alignment detection method that integrates YOLO object recognition, Devernay subpixel edge detection, and the RANSAC fitting algorithm. By employing both linear and elliptical fitting techniques, the method accurately determines the median line of the primary packaging container, ensuring precise alignment detection. The effectiveness of this approach is demonstrated by an average alignment distance of 0.28 mm with a standard deviation of 0.03 mm in lunar surface images, underscoring its accuracy and reliability.

Keywords: alignment detection; primary packaging container; median line; region of interest

1. Introduction

The Chang'e-6 lunar surface sampling mission, completed on June 25, 2025, as part of China's "Lunar Exploration Program," represents a significant milestone in space exploration, marking the first time humanity has successfully collected and returned samples from the Moon's far side [1]. This mission required overcoming several obstacles due to the unique challenges posed by the Moon's far side, including the inability to directly communicate with ground personnel. As a result, the Chang'e-6 mission relied heavily on advanced autonomous capabilities, including perception, analysis, judgment, and decision-making, to achieve its objectives. Among these capabilities, the precise alignment between the primary packaging container, which held the lunar soil samples, and the Chang'e-6 spacecraft was critical. The alignment process relied on a sampling surveillance system, where the camera was positioned to monitor the alignment between the primary packaging container and the sealed container. As shown in Figure 1a, the camera was mounted at a fixed angle to capture real-time images of the containers, ensuring that alignment detection could be performed with high accuracy. After the sampling, it was essential that the primary packaging container was correctly aligned with the sealed container attached to Chang'e-6 to ensure successful retrieval of the lunar soil. As shown in Figure 1b, the primary packaging container was detached from the top displacement device through a controlled explosive release, causing it to rapidly and forcefully descend into the sealed container below. If the alignment was not precise, this violent movement could cause a

failure in the drilling and sampling tasks. Therefore, the alignment detection of the primary packaging container is crucial to ensuring the success of the mission.
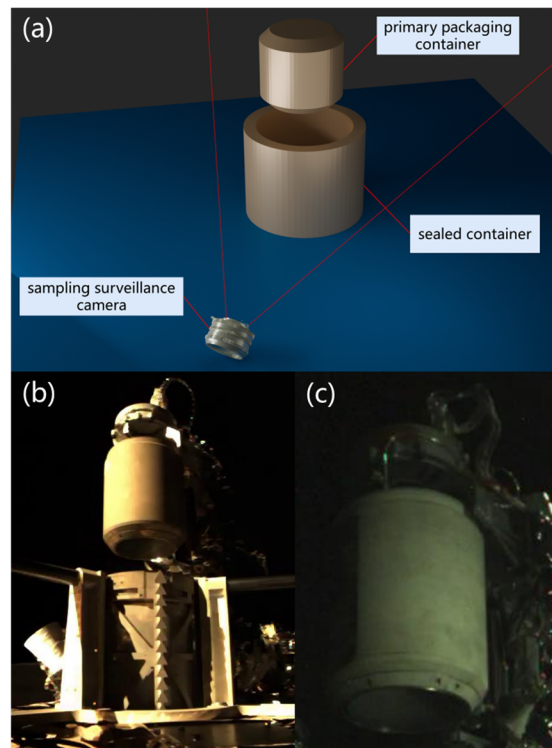
Figure 1. (**a**) Schematic diagram of hardware setup for alignment detection. (**b**) Primary packaging container and sealed container. (**c**) Hole in primary packaging container.

The primary packaging container was not directly inserted into the sealed container. Instead, it detached from the top displacement device through a controlled release and then descended into the sealed container. This required the alignment detection system on Chang'e-6 to be both highly accurate and stable, with a maximum permissible alignment error of 0.5 mm and a stability threshold of no less than 0.1 mm.

Several factors complicate the alignment detection process. Firstly, images captured often have complex backgrounds, with the region of interest (ROI) representing only a small portion, making it challenging to maintain the accuracy and stability of alignment detection due to potential background interference. Secondly, variations in the rotation angle of the primary packaging container can affect edge detection, as illustrated in Figure 1c. Thirdly, the Moon's surface reflects light unpredictably, introducing numerous uncertainties into the captured images due to the complex interactions between the camera and the reflective surfaces. To address the challenge, the alignment detection system relies on both natural sunlight and independent light sources. These light sources ensure reliable illumination in areas that may be in shadow or lack sufficient sunlight, allowing the system to continue operating effectively under varying lighting conditions. Finally, the three-dimensional nature of the task is challenging to interpret in two-dimensional images, especially when the container moves toward or away from the camera, which can impact the alignment detection's precision and stability.

While there have been some studies on alignment detection, they are often not fully applicable to the specific challenges faced by Chang'e-6. For example, Jose Lezama et al. developed a two-dimensional point pair alignment detection algorithm that is effective in noisy backgrounds but suffers from redundant calculations in complex environments [2], resulting in longer computation times and lower robustness due to its sensitivity to image variations. Zhang et al. proposed a joint alignment detection method using a multi-task

cascaded convolutional network [3], which offers improved detection performance and real-time capability but is highly sensitive to hyperparameters. Similarly, Sebastiano Battiato et al. presented a robust image alignment detection method based on image hashing [4], which is efficient and robust for detecting image transformations but unsuitable for object alignment within an image.

In light of these challenges, this paper introduces a novel alignment detection technique specifically tailored to the Chang'e-6 mission. In complex backgrounds, a deep convolutional neural network [5] is employed to accurately identify regions of interest, thereby enhancing target detection robustness. For scenarios involving the primary packaging container's structural holes, traditional edge detection methods [6–8] are combined with an elliptical fitting median line method [9] to improve accuracy. To address issues arising from reflective surfaces, an adaptive algorithm selection strategy for alignment detection is implemented. Furthermore, to manage dimensionality challenges when the container moves, a size ratio-based dimension expansion method is utilized. This comprehensive approach to alignment detection significantly improves accuracy, efficiency, and stability. Experimental results demonstrate that the proposed technique precisely calculates the distance and angle between the primary packaging container and the median line of the sealed container, ensuring precise alignment. The accuracy and stability achieved with this technique not only meet but exceed mission requirements, outperforming traditional methods.

2. Approach

In the Chang'e-6 mission, addressing the challenges posed by complex lunar images, as outlined in the introduction, requires precise extraction of two regions of interest (ROI): the primary packaging container and the sealed container. These challenges include background interference, unpredictable lighting conditions, and the three-dimensional nature of the task. To overcome these issues, several methods have been proposed to ensure accurate detection and alignment. Leonardo Rossi et al. introduced a novel ROI extraction layer that aims to overcome the limitations of traditional ROI extractors, which typically select only a single optimal layer from the feature pyramid network for feature extraction [10]. However, their model is hindered by high computational complexity and difficulties in hyperparameter tuning. Similarly, G. Rafiee et al. developed a two-stage unsupervised segmentation strategy using ensemble clustering and Gaussian difference methods to efficiently extract ROI from low depth-of-field images [11]. This method, however, struggles with errors when applied to images with complex backgrounds. Liu et al. suggested an ROI extraction technique based on the HSV color space and stereo vision, which quickly identifies salient regions by evaluating their saliency and refining the boundaries, all while minimizing computational complexity [12]. Despite its efficiency, this algorithm is sensitive to illumination changes and lacks robust generalization. In contrast, the YOLO (You Only Look Once) algorithm [5,13–15] has shown outstanding accuracy and robustness in ROI extraction, making it the preferred choice for object detection in this mission.

To address the issue of holes appearing in images captured during the rotation of primary packaging containers—which can lead to errors in image edge extraction and render traditional line fitting methods ineffective—a new approach has been developed. This technique specifically targets the unique features of these images, extracting the median line through bottom ellipse fitting of the primary packaging containers. Unlike previous methods, this approach remains robust even with container rotation, ensuring greater accuracy and reliability.

The lunar backlighting environment adds further complexity by creating multiple reflection points within images, which can compromise the accuracy of alignment detection. However, the bottom ellipse of the primary packaging container is relatively unaffected by these reflections, making it an effective reference for alignment detection. Despite this, the brightness of the bottom ellipse is typically lower and noisier than that of the side edge, which can reduce the accuracy of using an ellipse fitting method compared to a straight line fitting method. Therefore, under standard conditions, a straight line fitting approach is generally preferred. To optimize the process, an algorithm has been designed to adaptively select the most appropriate fitting method. This algorithm evaluates the presence of reflections and holes in the images to determine whether a straight line or ellipse fitting method is more suitable for each situation.

Furthermore, this paper addresses the challenge of detecting minor changes in two-dimensional images when the primary packaging container moves along the camera's optical axis, with the relative position of the sealed container and the camera remaining unchanged. In such cases, the size ratio between the primary and sealed containers in the image can be used to calculate their median line alignment in the optical axis direction.

The detection technology process developed for the Chang'e-6 mission is illustrated in Figure 2. This process primarily includes YOLO object recognition, line fitting for median lines, ellipse fitting for median lines, and the adaptive selection of the appropriate median line fitting algorithm.
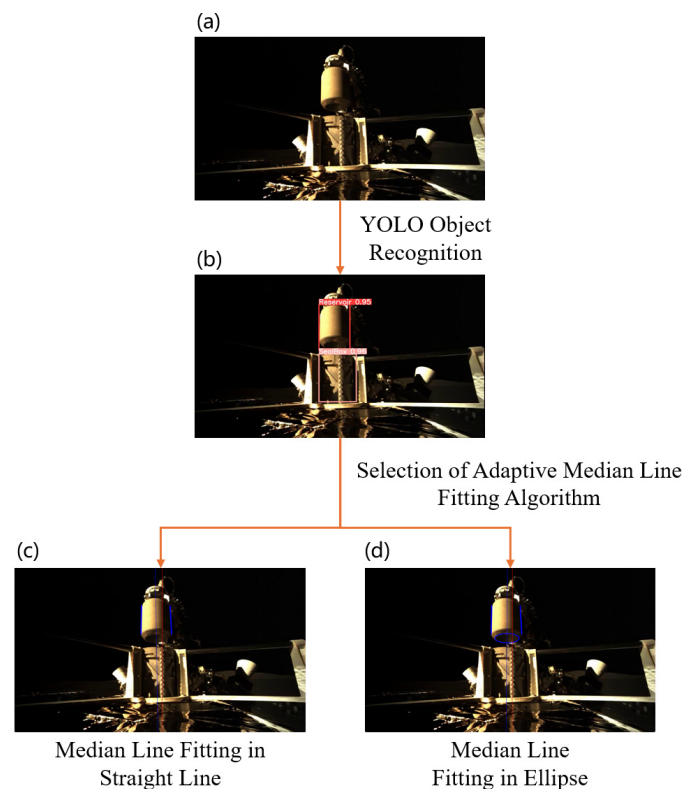
Figure 2. Schematic diagram of the algorithm. (**a**) Real image of Chang'e-6. (**b**) YOLO object recognition image. (**c**) Median line fitting result in straight line. (**d**) Median line fitting result in ellipse.

2.1. YOLO Object Recognition

The YOLO algorithm is designed to predict both the bounding box location and category probability of objects directly from input images using a deep convolutional neural network [14]. This approach allows for rapid object detection while maintaining high accuracy.

In applying the YOLO algorithm for object recognition, preprocessing the input image is essential. This step involves resizing and normalizing the image to match the model's input specifications. Once preprocessing is complete, the image undergoes feature extraction through a deep convolutional neural network. The model then generates a tensor that contains bounding box data, including predicted position, width, height, confidence level for each grid cell, and class probability. This bounding box information is subsequently decoded to transform the coordinates from the network's output space back to the original image's coordinate space. In the final step, the Non-Maximum Suppression (NMS) algorithm [16,17] is employed to refine the decoded bounding boxes by removing any overlapping or redundant ones. The refined bounding boxes, along with their class probabilities, are then provided as the final detection results.

Over time, the YOLO algorithm has evolved, with the latest version, YOLOv5, offering improved speed and accuracy over earlier iterations [14]. YOLOv5 also features enhanced universality and scalability, along with better multi-scale detection capabilities. Its streamlined design makes it an ideal choice for extracting regions of interest.

For the Chang'e-6 alignment detection task, the YOLOv5 algorithm is used to tackle the challenges posed by complex image backgrounds and small regions of interest. This method enables efficient extraction of the areas corresponding to the primary packaging container and the sealed container, reducing the computational load of the subsequent median line fitting process. As a result, both the accuracy and processing speed of the alignment detection are improved. The model is trained on multiple sets of images, captured under various conditions. Specifically, part of the training data was obtained from laboratory tests conducted on Earth, while the rest came from actual lunar surface operations during the Chang'e-5 mission. These images were used to train the model before the Chang'e-6 mission, and the training was completed on Earth prior to the mission launch. The detection results for the primary packaging container and sealed container from this model are then applied to actual images, as shown in Figure 3a.
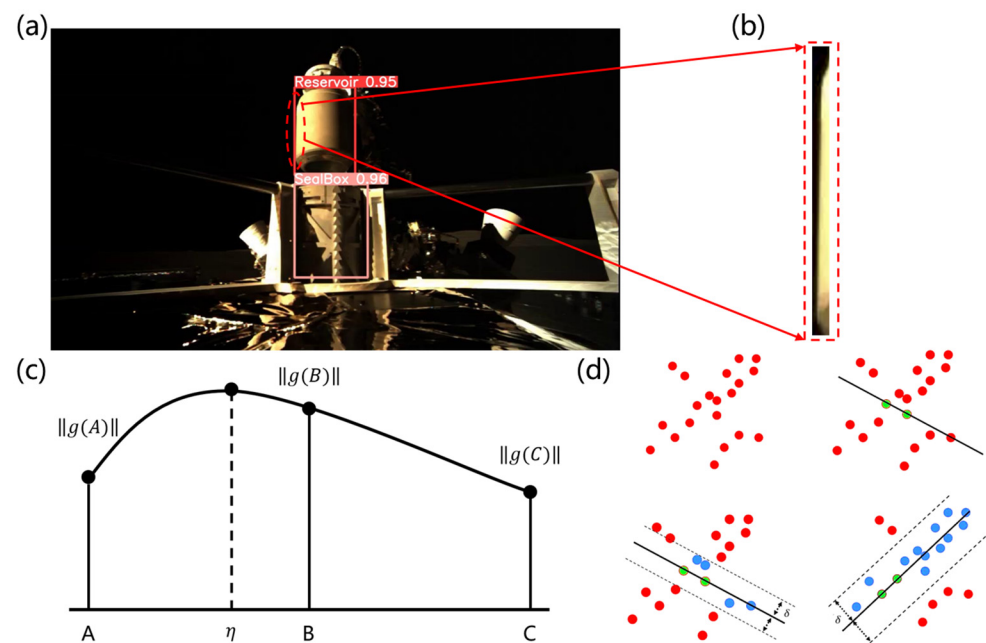
Figure 3. Schematic diagram of the algorithm. (**a**) Processing result of the YOLO algorithm. (**b**) Long strip-shaped region of interest. (**c**) Principal diagram of the Devernay subpixel edge extraction algorithm. (**d**) Simplified schematic diagram of the RANSAC algorithm.

2.2. Median Line Fitting in Straight Line

Since both the primary and sealed packaging containers are cylindrical, the position of the median line can be determined by isolating the left and right edges of the container and analyzing their positions. Within the region of interest identified by the YOLO algorithm, there may be additional edges on the container that could interfere with the extraction of the left and right edges. To improve the precision of edge extraction, a narrower, strip-shaped region of interest can be selected near the positions of the left and right edges within the original region of interest. This strategy effectively minimizes the impact of other container edges, as shown in Figure 3b.

Within this refined region of interest, a subpixel edge extraction algorithm is first employed to extract edges with greater precision. Although other methods, such as the partial area effect approach by Trujillo et al. [18] and Zernike moments [19], are promising for subpixel edge detection, we chose the Devernay subpixel edge extraction algorithm [20] due to its high accuracy and suitability for our engineering application. The Devernay algorithm has shown reliable performance in achieving subpixel edge detection accuracy in lunar surface images, meeting the precision requirements for the Chang'e-6 mission. Next, the RANSAC algorithm [21,22] is used to fit the potential edge points into a straight line, allowing for the optimal calculation of edge line parameters. Finally, using the two edge line parameters of the container, the median line parameters are computed.

The Devernay algorithm identifies edge points based on the maximal gradient modulus difference between adjacent points. It works by interpolating a quadratic function of the gradient modulus at three nearby points along the gradient direction, as illustrated in Figure 3c. While this method provides the necessary accuracy for the task, its computational cost can be high. To mitigate this, an approximate formula can be used to simplify the fitting process without compromising edge detection precision:

$$\eta = \frac{1}{2} \frac{\|g(A)\| - \|g(C)\|}{\|g(A)\| + \|g(C)\| - 2\|g(B)\|},\tag{1}$$

where $\|g(A)\|$, $\|g(B)\|$ and $\|g(C)\|$ represent the gradient magnitudes at three points, and η is the maximum difference in gradient magnitude.

After extracting the subpixel edge points, these points need to be fitted into edge lines. The least squares method, however, often results in significant errors when fitting edge lines due to its sensitivity to image noise and background interference. To address this, the RANSAC line fitting algorithm is used for a more accurate approach [21,22]. As shown in Figure 3d, the RANSAC line fitting algorithm begins by randomly selecting two points (green points) from the candidate subpixel edge points (red points) and fitting a line using these points. The distances of all other candidate edge points to this line are then calculated. Points within a predefined threshold distance (illustrated by the dashed boundary) from the line are considered inliers (blue points). This process is repeated multiple times, with the number of iterations set beforehand. The model that accumulates the highest number of inliers is selected, and all inliers within this model are used for least squares line fitting to derive the optimal edge. This iterative process ensures robustness against outliers (red points outside the dashed boundary), leading to a more accurate line fitting result.

By applying Devernay subpixel edge detection and RANSAC line fitting techniques, the median line of both the primary and sealed containers is derived, as illustrated in Figure 4a, where the blue line represents the median line fitted to the primary packaging container, and the red line represents the median line fitted to the sealed container.
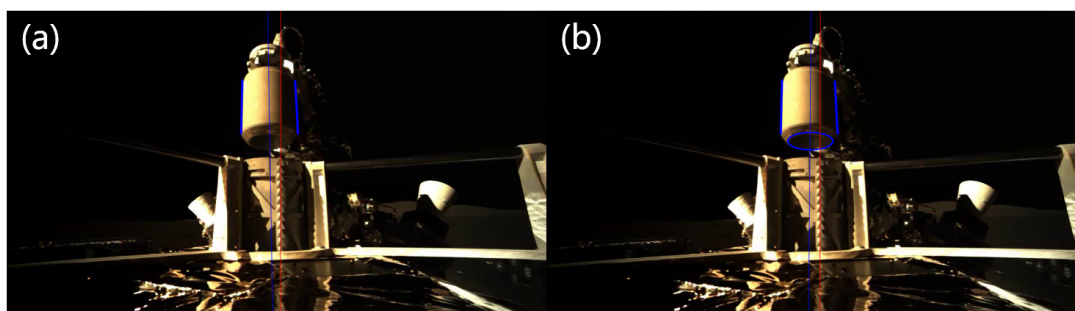
Figure 4. (**a**) Results of the line fitting median. (**b**) Results of the ellipse fitting median.

2.3. Median Line Fitting in Ellipse

During the rotation of the primary packaging container, holes may appear in the elongated region of interest, leading to significant errors when fitting the midline with a straight line. To ensure accurate midline fitting, alternative methods must be considered. Since the round bottom of the primary packaging container appears as an ellipse in the image, the ellipse's minor axis can be used to represent the midline of the primary packaging container.

Within the region of interest identified by the YOLO algorithm, elliptical template matching is used to extract sub-regions of interest. This approach helps avoid interference from other edges during the initial fitting of the bottom ellipse of the primary packaging container. In the refined region, a subpixel edge extraction algorithm is employed to accurately delineate the ellipse's edges. Then, the RANSAC algorithm [22] is used to align the potential edge points into an elliptical shape, deriving the optimal elliptical parameters. These parameters are then used to calculate the ellipse's minor axis, which serves as the baseline for the primary packaging container.

For inlier filtering in the RANSAC algorithm, a threshold is determined by the weighted average of distances from each point to the focus. Points located at a distance less than this threshold are classified as inliers. The initial focus is provided by the results of YOLO object recognition, and the weight assigned to each potential edge point is calculated based on the sum of distances from each point to the initial focus:

$$w_i = e^{-\frac{1}{2}|2a_0 - r_{0i}|},\tag{2}$$

where a_0 is the prior semi-major axis length, and w_i is the weight of each candidate edge point.

In cases where images of the primary packaging container show holes, the results derived from the median line of both the primary and sealed containers are shown in Figure 4b. These results are obtained using Devernay subpixel edge detection and RANSAC ellipse fitting techniques.

2.4. Selection of Adaptive Median Line Fitting Algorithm

For the Chang'e-6 mission, an automated approach to selecting the optimal median line fitting algorithm is essential to handle scenarios prone to significant errors, such as holes, uneven illumination, and reflections. To address these challenges, gamma correction is first applied to the image to standardize illumination across the scene. Next, the mean and variance of the grayscale values within the elongated region of interest, shown in Figure 3b, are calculated.

When the image of the primary packaging container exhibits holes or intense reflections, the mean and variance of the grayscale values will be either unusually high or

low. By setting dual thresholds for these metrics, the system can automatically identify such anomalies.

During the initial assessment of the primary packaging container, the system calculates the mean and variance of the grayscale values within the specified elongated region of interest. These values are then compared to predetermined thresholds. If both metrics are within the acceptable range, a line fitting median is selected; otherwise, an ellipse fitting median is applied. This adaptive method ensures accurate alignment detection, regardless of the varying conditions of the images.

3. Experiment

To evaluate the effectiveness of the alignment detection algorithm, experiments were conducted using images of the primary packaging container captured in two different environments: a simulated lunar surface and the actual far side of the moon. The objective was to assess the algorithm's performance under various conditions.

The experimental data is categorized into two parts. The first part consists of images obtained from Chang'e-6 on a simulated lunar surface, primarily used for training the YOLO model, designing initial algorithms for alignment detection, and evaluating the accuracy, precision, and robustness of the detection functions. The second part includes real images taken on the actual lunar surface.

### 3.1. Simulation of Lunar Surface Experiment

To test the alignment detection algorithm's effectiveness and robustness, parameters such as the position, rotation angle, and light intensity of the primary packaging container were varied. The tests were conducted on Earth in a simulated lunar environment at the Aerospace Research Institute's dedicated test facility. The test environment simulated various lunar conditions, including lunar soil simulation, terrain types, and drilling and sampling conditions. These simulations were designed to closely mimic the physical properties of the lunar surface and the challenges faced during actual lunar operations.

First, the impact of rotation angle on alignment detection performance was examined under consistent location and lighting conditions. The primary packaging container was rotated completely, with images captured at each position for alignment detection. These results are shown in Figure 5. An image taken at the precise alignment moment was used as the baseline. By calculating the difference between the angle and distance of the primary packaging container relative to the median line within the sealed container in each test image, compared to the baseline image, the alignment detection results were obtained, as detailed in Table 1.

Table 1. Impact of Different Rotation Angles on the Alignment Detection Results in Primary Packaging Container.

Serial Number	Angle (rad)	Distance (mm)
1	0.002	0.17
2	0.002	0.17
3	0.001	0.12
4	0.001	0.12
5	0.001	0.15
6	0.001	0.18
7	0.001	0.13
8	0.001	0.15
9	0.002	0.12
10	0.001	0.14
11	0.001	0.13
12	0.002	0.17
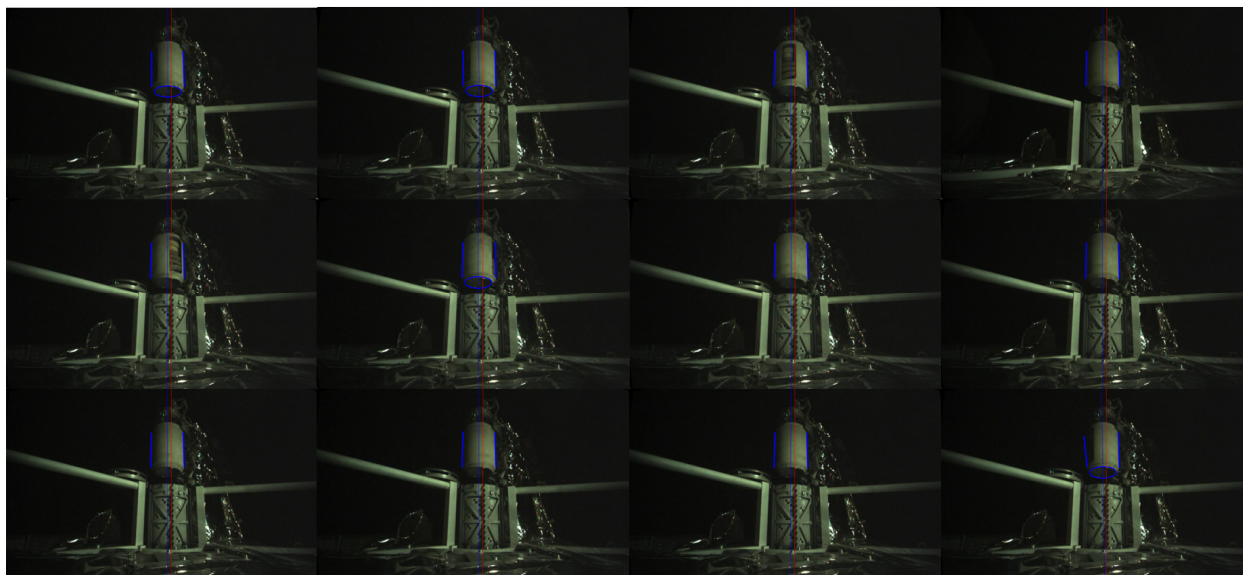
Figure 5. Comparison of alignment detection results at different rotational angles of the primary packaging container.

Analysis of 12 sets of image data revealed a mean value for the angle of 0.001 rad with a standard deviation of 0.001 rad. The mean value for the distance was 0.15 mm, with a standard deviation of 0.02 mm. These results suggest that, under consistent positioning and lighting conditions, the alignment detection algorithm exhibits high precision and stability with respect to rotation angle. This demonstrates the algorithm's effectiveness in addressing issues such as holes appearing in primary packaging containers during rotation.

Next, the effect of varying light intensities on alignment detection performance was evaluated under fixed position and rotation angle conditions. In this experiment, the primary packaging container remained stationary while the ambient light intensity was altered. Images were captured at different light intensities for alignment detection, as shown in Figure 6. The angle and distance between the primary packaging container and the median line within the sealed container were calculated for each test image and compared to the baseline image results, as outlined in Table 2.

Analysis of 6 sets of image data showed that the mean value for the angle was 0.001 rad with a standard deviation of 0.001 rad. The mean value for the distance was 0.14 mm, with a standard deviation of 0.03 mm. These findings indicate that under consistent position and rotation angle conditions, the alignment detection algorithm is highly precise and robust to variations in light intensity. Moreover, the algorithm performs effectively even in low-light environments, successfully handling uneven lighting and reflections commonly encountered with primary packaging containers.

Table 2. Impact of Different Light Intensities of Alignment Detection Results in Primary Packaging Container.

Serial Number	Angle (rad)	Distance (mm)
1	0.001	0.10
2	0.001	0.11
3	0.001	0.15
4	0.002	0.17
5	0.002	0.16
6	0.001	0.15
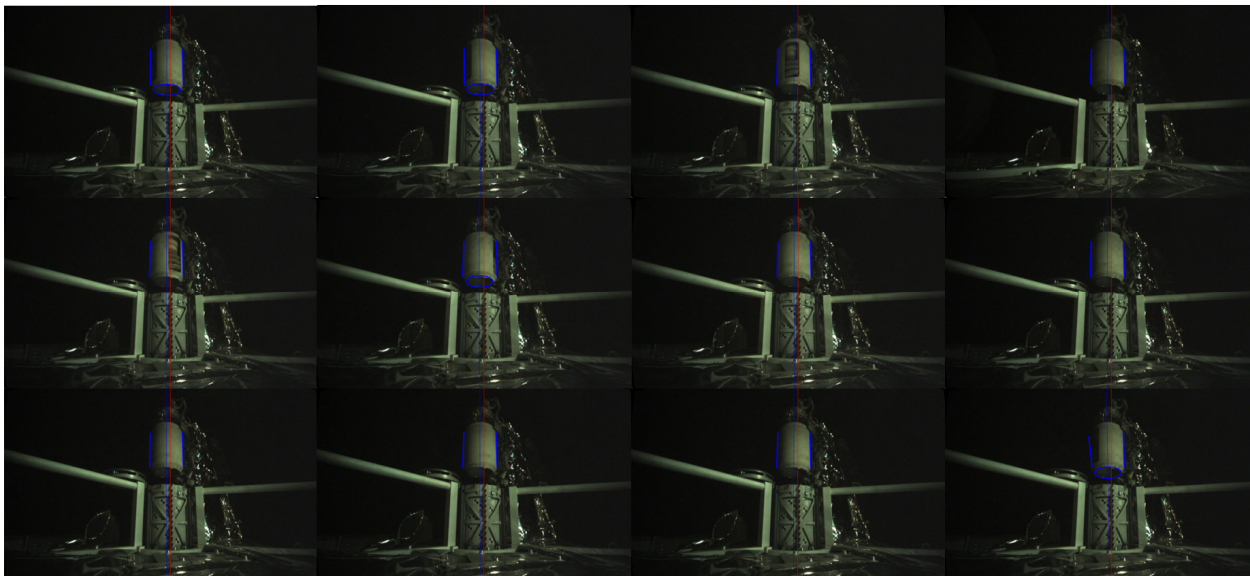
Figure 6. Comparison of alignment detection results at different light intensities of primary packaging container.

3.2. Practical Lunar Surface Results

During the Chang'e-6 mission on the far side of the Moon, the alignment detection algorithm was employed to analyze images captured during the sampling process. To ensure accuracy and reliability, multiple images were used for testing. The Chang'e-6 sampling surveillance camera captured 12 images during the actual sampling procedure. The results from the alignment detection algorithm are shown in Figure 7, and the alignment detection outcomes relative to the benchmark are detailed in Table 3.
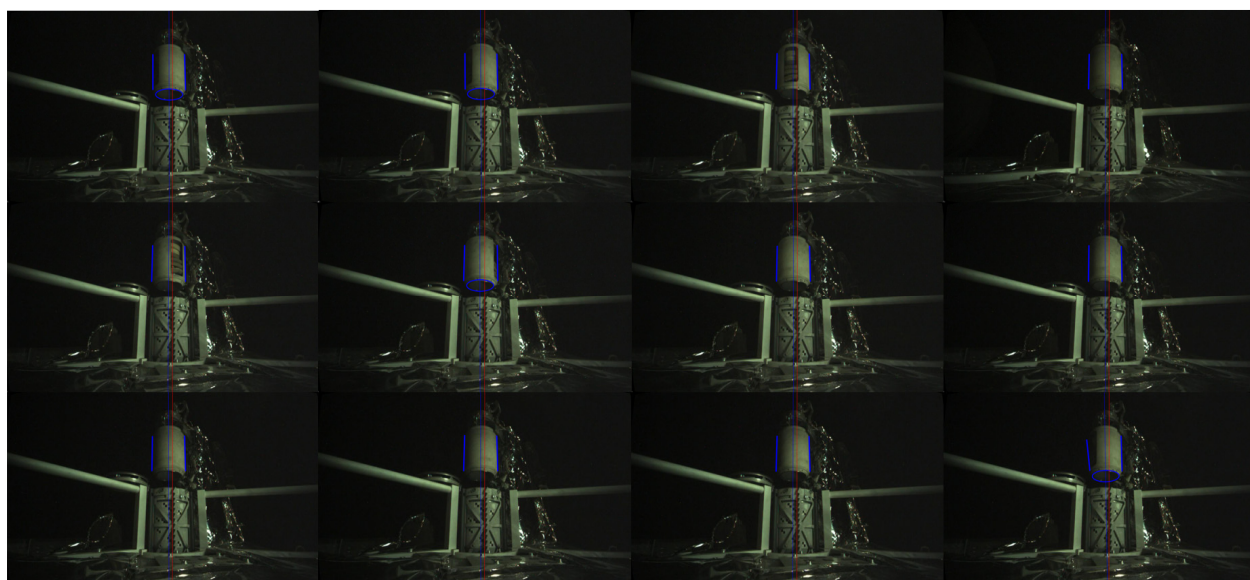
Figure 7. Alignment detection results from Chang'e-6's lunar mission.

Analysis of the actual image alignment detection results indicated that no holes were present in the primary packaging container during sampling. However, due to uneven lighting conditions, the right side of the container appeared darker, leading to less accurate edge detection. As a result, the method of fitting the median line using the elliptical base of the primary packaging container was chosen over the straight-edge fitting method.

Table 3. Impact of Different Conditions on Alignment Detection Results in Primary Packaging Container.

Serial Number	Angle (rad)	Distance (mm)
1	0.001	0.29
2	0.002	0.28
3	0.003	0.22
4	0.003	0.25
5	0.003	0.27
6	0.003	0.29
7	0.001	0.32
8	0.001	0.28
9	0.001	0.29
10	0.001	0.28
11	0.001	0.29
12	0.001	0.32

Analysis of 12 sets of image data revealed a mean orthogonal angle of 0.002 rad with a standard deviation of 0.001 rad. The mean orthogonal distance was 0.28 mm, with a standard deviation of 0.03 mm. These results suggest that the alignment detection algorithm achieves high precision and stability in actual lunar surface environments, with detection accuracy not less than 0.5 mm and stability not less than 0.1 mm, thus meeting task requirements. However, due to uncontrollable factors present in field images of the lunar surface, the accuracy is slightly lower than that achieved in simulated lunar environments.

The successful application of this detection technology enabled precise alignment detection of the primary packaging container and sealed container after Chang'e-6 sampled on the far side of the Moon, marking the successful completion of the mission.

4. Conclusions

To meet the alignment requirements and address the practical challenges of the primary packaging container in the Chang'e-6 lunar surface autonomous sampling mission, we developed a detection technique that combines both linear and elliptical midline fitting methods. This technique leverages YOLO target recognition on images captured by the Chang'e-6 sampling surveillance camera to identify and extract regions of interest for the primary and sealed containers. By analyzing grayscale mean and variance against dual thresholds, the method determines whether to employ linear or elliptical midline fitting. Edge extraction is then performed within these regions, and the parameters are derived using RANSAC fitting, either linear or elliptical. These parameters are used to calculate the midlines of the primary and sealed containers, which are compared to a reference image to evaluate their relative angles and distances. This process ensures precise container alignment and facilitates the adjustment of the primary packaging container for optimal alignment.

The algorithm's performance was assessed using images from both a simulated lunar surface and the actual far side of the Moon. For the real lunar surface images, the mean corrected angle was 0.002 rad with a standard deviation of 0.001 rad, and the mean corrected distance was 0.28 mm with a standard deviation of 0.03 mm. These results confirm that the algorithm achieves the necessary precision and stability, demonstrating its effectiveness and reliability for alignment detection in both simulated and real lunar environments.

References

1. Zeng, X.; Liu, D.; Chen, Y.; Zhou, Q.; Ren, X.; Zhang, Z.; Yan, W.; Chen, W.; Wang, Q.; Deng, X.; et al. Landing site of the Chang'e-6 lunar farside sample return mission from the Apollo basin. *Nat. Astron.* **2023**, *7*, 1188–1197. [CrossRef]
2. Lezama, J.; Morel, J.-M.; Randall, G.; von Gioi, R.G. A contrario 2d point alignment detection. *IEEE Trans. Pattern Anal. Mach. Intell.* **2014**, *37*, 499–512. [CrossRef] [PubMed]
3. Zhang, K.; Zhang, Z.; Li, Z.; Qiao, Y. Joint face detection and alignment using multitask cascaded convolutional networks. *IEEE Signal Process. Lett.* **2016**, *23*, 1499–1503. [CrossRef]
4. Battiato, S.; Farinella, G.M.; Messina, E.; Puglisi, G. Robust image alignment for tampering detection. *IEEE Trans. Inf. Forensics Secur.* **2012**, *7*, 1105–1117. [CrossRef]
5. Bochkovskiy, A.; Wang, C.Y.; Liao, H.Y.M. Yolov4: Optimal speed and accuracy of object detection. *arXiv* **2020**, arXiv:2004.10934.
6. Canny, J. A computational approach to edge detection. *IEEE Trans. Pattern Anal. Mach. Intell.* **1986**, *8*, 679–698. [CrossRef] [PubMed]
7. Ziou, D.; Tabbone, S. Edge detection techniques-an overview. *Распознавание Образов Анализ Изображен/Pattern Recognit. Image Anal. Adv. Math. Theory Appl.* **1998**, *8*, 537–559.
8. Maini, R.; Aggarwal, H. Study and comparison of various image edge detection techniques. *Int. J. Image Process. (IJIP)* **2009**, *3*, 1–11.
9. Stojmenovic, M.; Nayak, A. Direct ellipse fitting and measuring based on shape boundaries. In *Advances in Image and Video Technology, Proceedings of the Second Pacific Rim Symposium, PSIVT 2007 Santiago, Chile, 17–19 December 2007*; Proceedings 2; Springer: Berlin/Heidelberg, Germany, 2007; pp. 221–235.
10. Rossi, L.; Karimi, A.; Prati, A. A novel region of interest extraction layer for instance segmentation. In Proceedings of the 2020 25th International Conference on Pattern Recognition (ICPR), Milan, Italy, 10–15 January 2021; IEEE: Piscataway, NJ, USA, 2021; pp. 2203–2209.
11. Raffee, G.; Dlay, S.S.; Woo, W.L. Region-of-interest extraction in low depth of field images using ensemble clustering and difference of Gaussian approaches. *Pattern Recognit.* **2013**, *46*, 2685–2699. [CrossRef]
12. Liu, Z.; Chen, W.; Zou, Y.; Hu, C. Regions of interest extraction based on HSV color space. In Proceedings of the IEEE 10th International Conference on Industrial Informatics, Beijing, China, 25–27 July 2012; IEEE: Piscataway, NJ, USA, 2012; pp. 481–485.
13. Redmon, J.; Divvala, S.; Girshick, R.; Farhadi, A. You only look once: Unified, real-time object detection. In Proceedings of the IEEE Conference on Computer Vision and Pattern Recognition, Las Vegas, NV, USA, 27–30 June 2016; pp. 779–788.
14. Jiang, P.; Ergu, D.; Liu, F.; Cai, Y.; Ma, B. A Review of Yolo algorithm developments. *Procedia Comput. Sci.* **2022**, *199*, 1066–1073. [CrossRef]
15. Ge, Z.; Liu, S.; Wang, F.; Li, Z.; Sun, J. Yolox: Exceeding yolo series in 2021. *arXiv* **2021**, arXiv:2107.08430.
16. Neubeck, A.; Van Gool, L. Efficient non-maximum suppression. In Proceedings of the 18th International Conference on Pattern Recognition (ICPR'06), Hong Kong, China, 20–24 August 2006; IEEE: Piscataway, NJ, USA, 2006; Volume 3, pp. 850–855.
17. Hosang, J.; Benenson, R.; Schiele, B. Learning non-maximum suppression. In Proceedings of the IEEE Conference on Computer Vision and Pattern Recognition, Honolulu, HI, USA, 21–26 July 2017; pp. 4507–4515.
18. Trujillo-Pino, A.; Krissian, K.; Alemán-Flores, M.; Santana-Cedrés, D. Accurate subpixel edge location based on partial area effect. *Image Vis. Comput.* **2013**, *31*, 72–90. [CrossRef]

19. Renshaw, D.T.; Christian, J.A. Subpixel localization of isolated edges and streaks in digital images. *J. Imaging* **2020**, *6*, 33. [CrossRef] [PubMed]

20. Devernay, F. *A Non-Maxima Suppression Method for Edge Detection with Sub-Pixel Accuracy*; INRIA: Le Chesnay-Rocquencourt, France, 1995.

21. Bolles, R.C.; Fischler, M.A. A RANSAC-based approach to model fftting and its application to ffnding cylinders in range data. In Proceedings of the IJCAI, Vancouver, BC, Canada, 24–28 August 1981; pp. 637–643.

22. Choi, S.; Kim, T.; Yu, W. Performance evaluation of RANSAC family. *J. Comput. Vis.* **1997**, *24*, 271–300.